NUMERICAL STUDY OF COLLAPSE BEHAVIOR OF STEEL BUILDINGS DUE TO EXTREMELY HIGH SEISMIC LOAD

Said ELKHOLY[1] and Kimiro MEGURO[2]

[1] Postdoctoral fellow, Institute of Industrial Science, The University of Tokyo
4-6-1 Komaba, Meguro-ku, Tokyo 153-8505, Japan, elkholy@risk-mg.iis.u-tokyo.ac.jp
[2] Professor, Institute of Industrial Science, The University of Tokyo
4-6-1 Komaba, Meguro-ku, Tokyo 153-8505, Japan, meguro@iis.u-tokyo.ac.jp

This paper focuses on the methodology for modeling the dynamic behavior of steel structures due to severe earthquake ground motions. The development of the Improved Applied Element Method for analyzing the entire behavior of large-scale steel structures up to total failure is briefly discussed. The main features of the method are illustrated. The presented case-studies show different collapse mechanisms of moment-resistance steel frame structure under severe ground motions. The results show high capability on simulating the observed damage of many steel structures due to recent earthquakes.

***Key words**: Numerical simulation, Improved Applied Element Method, AEM, Collapse, Earthquake Damage, Progressive Failure*

1. INTRODUCTION

Starting in the 1960s, welded steel moment-resisting frame buildings have been regarded as being among the most ductile systems contained in the building code. Prior to Northridge Earthquake (1994), it had been believed that steel moment-resisting-frame buildings were essentially invulnerable to earthquake-induced structural damage and thought that should such damage occur, it would be limited to ductile yielding of members and connections (FEMA[1)]). The 1994 Northridge earthquake caused serious damage to modern steel structures. The brittle fractures of beam-to-column connections for the moment-frame buildings were widely observed (Miller[2)]). The damaged buildings were of various heights ranging from one story to 26 stories. One year later, in the Kobe earthquake (1995), nearly one thousand steel buildings were damaged, as well as 90 buildings being collapsed, 333 buildings being severely damaged, and 300 being slightly damaged (Nakashima[3)] and Holguin[4)]). According to the FEMA report[1)], modern steel-frame buildings, specially constructed to sway rather than fracture during an earthquake, are more vulnerable to collapse than had ever been considered. A poor design could cause these often massive skyscrapers to crack, tilt and even collapse during violent shaking. To reduce such damage, it is important to understand its main mechanism. However, it is very difficult or practically impossible to perform damage tests for total collapse process of real scale steel structures, especially high rise buildings. Therefore, studying those phenomena requires powerful numerical tools that can extend the analysis up to complete failure.

To obtain full knowledge of the total behavior of steel structures under severe ground motions, it is essential to simulate the collapsing process and the trace of yielding and deformation at each structural member. The reliable numerical models are highly required as a cost effective method of obtaining a comprehensive knowledge of the main parameters that affect response of structures under severe earthquakes. The advanced analytical methods enable engineers to predict the type and range of possible collapse in both the design stage and after incidents to enhance the safety of people in structures. For that reason, recently, a significant amount of research works has been carried out to considerable research efforts dealing with collapse analysis have been developed such as Rigid Bodies Spring Model (RBSM)[5], Extended Distinct Element Method (EDEM)[6], combined FEM/DEM[7], and Applied Element Method (AEM)[8~10]. Nevertheless, none of them have yet been used for collapse analysis of steel structures. In order to guarantee decent accuracy of the solution in the case of modeling of steel structure using AEM, a very large number of elements will be required to extend the computer power and time needed for numerical simulation.

Therefore, In this paper the formulations of Improved Applied Element Method (IAEM)[11~13] are presented, where the effects of geometric and material nonlinearities are considered. The main features and analysis capabilities of IAEM are discussed, and verification examples are performed to demonstrate the extreme efficiency of the developed code in performing inelastic analysis for steel structures. The IAEM requires a very small number of degrees of freedom compared to conventional AEM, while decreasing the CPU time needed for analysis and increasing the capacity of the solver. A case study shows the different collapse mechanisms of a nine-story steel structure model under severe ground motion excitations. The proposed method can be utilized to achieve better understanding of the response of structures toward ground motion, impact, fire, and hazardous blasting.

2. APPLIED ELEMENT METHOD

Only a brief introduction to the two-dimensional Applied Element Method is given here. The AEM is a recently developed technique for structural analysis (Meguro[8]). The application of AEM to structural analysis is recognized as a powerful tool for analyzing the structural behavior from early stage of loading and up to the total collapse occurs (Tagel-Din[10]).

In AEM, the structure is modeled as an assembly of small rigid square elements. In two dimensions analysis, each element has three degrees of freedom. A pair of elements is connected with pairs of normal and shear springs uniformly distributed on the boundary line. Each pair of springs totally represents stresses and deformations of a certain area (hatched area in **Figure 1**) of the studied elements. Therefore, the normal and shear stiffness can be determined by Equation 1.

$$K_n = \frac{E \times d \times T}{a} \quad \text{and} \quad K_S = \frac{E \times d \times T}{a} \qquad (1)$$

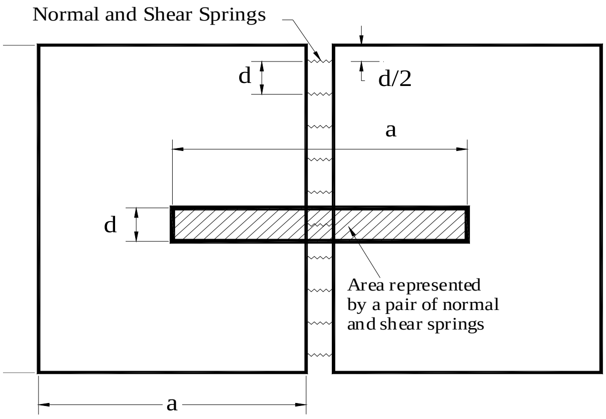

Figure 1 Area of influence of each pair of springs

where d is distance between each spring; a is length of representative area; *E* and *G* are Young's and shear modules of the material, respectively; and *T* is the thickness of element, which is considered constant for all springs attached to the element (Meguro [8]).

The springs represent the microscopic material properties, such as stiffness and yield strength. The conventional AEM used in different engineering field has shown high accuracy and applicability for modeling reinforced concrete[10], soil[14] and masonry[15]. However, some applications are difficult to handle like huge steel structure buildings. Using the current version of AEM, elements with very small size should be used to follow the change in the thickness especially in non-rectangle cross sections (i.e. I Shape, Channel, and Boxed sections), since the element should be chosen to fit the flange thickness. In this paper, we introduce the Improved Applied Element Method which can easily handle this type of cases.

3. IMPROVED APPLIED ELEMENT METHOD (IAEM)

(1) Basic formulations

IAEM is a newly developed method for structural analysis of large scale structural[11~13]. It can follow total behavior of structures up to complete failure stage with high accuracy in reasonable CPU. In IAEM, each structural member is divided into a proper number of rigid elements connected by pairs of normal and shear springs uniformly distributed on the boundary line between elements. Two major extensions of the AEM[8] have been implemented in IMEM: The first is improving the element type to use different thickness per each spring to be able to follow change of thickness in non-rectangular cross-sections. The second is using different thicknesses for calculating normal stiffness and shear stiffness in each pair of springs. These modifications allow modeling cross sectional geometric parameters of structural members using elements with large size. The value of normal and shear stiffness for each pair of springs can be determined as:

$$K_n^i = \frac{E \times d \times T_n^i}{a} \quad \text{And} \quad K_s^i = \frac{E \times d \times T_s^i}{a} \qquad (2)$$

where: d is the distance between each spring; a is the length of the representative area; E and G are Young's and shear modules, respectively; T_n^i and T_s^i are the thickness represented by the pair of springs "i" for normal and shear cases, respectively.

A pair of rigid elements, as shown in **Figure 2**, are assumed to be connected by only one pair of normal spring stiffness (K_n^i) and shear spring stiffness (K_s^i). The values of dx and dy correspond to the relative coordinate of the contact point with respect to the center of gravity. To have a global stiffness matrix, the location of elements and contact springs is assumed in a general position. The stiffness matrix components corresponding to each D.O.F. are determined by assuming a unit displacement in the studied direction and by determining forces at the centroid of each element. The element stiffness matrix size is only (6 x 6). Equation (3) shows the components of the upper left quarter of the stiffness matrix. All notations used in this equation are shown in **Figure 2**.

$$\left[\begin{array}{l|l|l}
\begin{array}{l} Sin^2(\theta+\alpha)K_n^i \\ +Cos^2(\theta+\alpha)K_S^i \end{array} & \begin{array}{l} -K_n^iSin(\theta+\alpha)Cos(\theta+\alpha) \\ +K_S^iSin(\theta+\alpha)Cos(\theta+\alpha) \end{array} & \begin{array}{l} Cos(\theta+\alpha)K_S^iLSin(\alpha) \\ -Sin(\theta+\alpha)K_n^iLCos(\alpha) \end{array} \\ \hline
\begin{array}{l} -K_n^iSin(\theta+\alpha)Cos(\theta+\alpha) \\ +K_S^iSin(\theta+\alpha)Cos(\theta+\alpha) \end{array} & \begin{array}{l} Sin^2(\theta+\alpha)K_S^i \\ +Cos^2(\theta+\alpha)K_n^i \end{array} & \begin{array}{l} Cos(\theta+\alpha)K_n^iLCos(\alpha) \\ +Sin(\theta+\alpha)K_S^iLSin(\alpha) \end{array} \\ \hline
\begin{array}{l} Cos(\theta+\alpha)K_S^iLSin(\alpha) \\ -Sin(\theta+\alpha)K_n^iLCos(\alpha) \end{array} & \begin{array}{l} Cos(\theta+\alpha)K_n^iLCos(\alpha) \\ +Sin(\theta+\alpha)K_S^iLSin(\alpha) \end{array} & \begin{array}{l} L^2Cos^2(\alpha)K_n \\ +L^2Sin^2(\alpha)K_S^i \end{array}
\end{array}\right] \qquad (3)$$

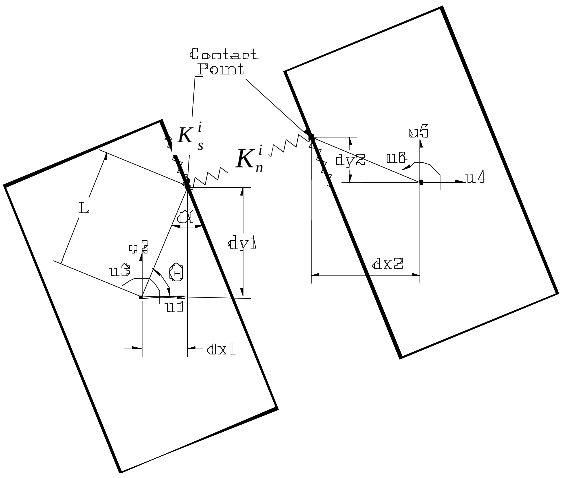

Figure 2 Contact Point and D.O.F

Although in this method, we can change the characteristics of all springs surrounding any element, in practice, only changing the corner springs is needed for steel flanged sections. As shown in **Figure 3**, changing the ratios of (K_1/K_2) and (K_3/K_4) can control the stiffness of any element. That kind of improvement allows using many different flanged steel sections like I-beam, Box and Channel cross sections. Moreover, any cross section can be simulated by adjusting the values of the element height, number of springs, ratio of outer to inner thickness, and the ratio of normal to shear thickness.

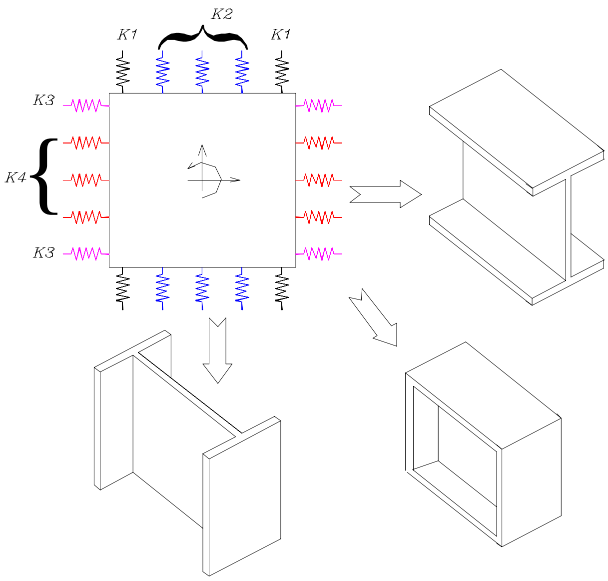

Figure 3 Element Shape for IAEM

(2) Dynamic analysis in IAEM

The general differential equation of motion, governing the response of structure in a small displacement range can be expressed as:

$$[M]\{\Delta\ddot{U}\}+[C]\{\Delta\dot{U}\}+[K]\{\Delta U\}=\Delta f(t)-[M]\{\Delta\ddot{U}_G\} \quad (4)$$

where: $[M]$ is mass matrix; $[C]$ is the damping matrix; $[K]$ is the nonlinear stiffness matrix; $\Delta f(t)$ is the incremental applied load vector; $\{\Delta\ddot{U}\},\{\Delta\dot{U}\},\{\Delta U\}$ and $\{\Delta\ddot{U}_G\}$ are the incremental acceleration, velocity, acceleration, and gravity acceleration vectors, respectively. The mass matrix and the polar moment of inertia of each element have been idealized as lumped at the element centroid. The lumped mass in each D.O.F direction can be calculated by summing the effect of small segmental masses represented by each spring considering the change of the springs' thickness. Equation (5) represents the value of lumped mass in each degree of freedom direction assuming that elements have rectangular shape.

$$\begin{bmatrix} M1 \\ M2 \\ M3 \end{bmatrix} = \begin{bmatrix} \frac{a\times b\times\rho}{nsp}.\sum_{i=1}^{i=nsp} t_i^x \\ \frac{a\times b\times\rho}{nsp}.\sum_{i=1}^{i=nsp} t_i^y \\ \frac{\rho}{nsp}\cdot\sum_{i=1}^{i=nsp}(\frac{t_i^x\times a^3\times b}{12\times nsp}+\frac{t_i^y\times a\times b^3}{12\times nsp}) \end{bmatrix} \quad (5)$$

where: a and b are the element dimensions; ρ the density of the material considered; nsp is the number of connecting springs, and t_i^x and t_i^y are the thickness of spring 'i' the element local directions.

(3) Geometric nonlinearity

The geometric nonlinearity due to large displacement has been introduced by Tagel-Din and Meguro[9]. According to their concept, the AEM can follow the geometric nonlinearity under both static and dynamic load by applying a slight change in the equation of motion Equation (6).

$$[M]\{\Delta\ddot{U}\}+[C]\{\Delta\dot{U}\}+[K]\{\Delta U\}=\Delta f(t)+R_m+R_G \quad (6)$$

where R_m represents the residual force vector due to cracking and incompatibility between strain and stress of each spring; and R_G the residual force vector due to geometrical changes in the structure during loading.

By assuming R_m and R_G equal to null and solving Equation (6) to get $\{\Delta U\}$, the geometry of the structure can be modified to obtain the direction of spring force vectors according to the new element configuration. From the incompatibility between the applied force and the internal stress the value of R_G is calculated. In case of considering the material nonlinearity, the material residual load vector R_m is calculated by checking the situation of cracking. However in case of elastic analysis R_m equals null.

(4) Material nonlinearity

Over previous decades, numerous researchers have developed and validated various methods of performing the inelastic analysis on steel frames based on second order inelastic analysis which can be categorized into two main approaches:

1) plastic hinge based approach which is considered the most direct and simplified approach for representing the material nonlinearity. In this model, all elements are assumed to remain elastic except at the places where zero length plastic hinges are allowed to form[16),17)]. This method accounts for inelasticity but it can't account for the spread of yielding through the section. Therefore, it is not possible to capture member stability with enough accuracy for a wide range of beam-to-column problems[18)].

2) Plastic zone analysis in which the spread of plasticity of the member is assumed to be modeled by subdividing the frame members into several finite elements. Furthermore, each element is subdivided into many fibers[19),20)]. The plastic zone solution is known as an exact solution. This method has been used in IAEM whereas the connecting springs work as fibers. Once the strain of each spring is calculated, the stress state can be explicitly determined and the gradual spread of yielding traced.

(5) Material Model

A simplified uniaxial bilinear stress-strain model with kinematic strain hardening is adapted for representing the normal stiffness component of structural steel, as shown in **Figure 4**. In this model, the plastic range remains constant throughout the various loading stages. Although, this is not an entirely realistic representation of the material behavior, it allows for the hardening to be included while keeping the formulation simple.

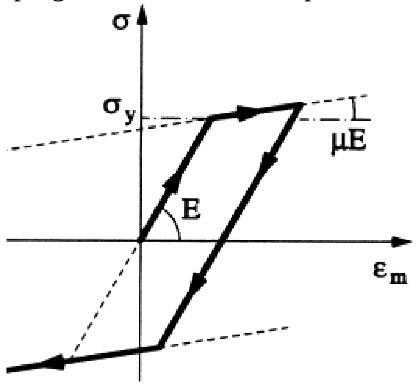

Figure 4 Material Model

4. VERIFICATIONS OF THE PROPOSED TECHNIQUE

Two examples are presented to demonstrate that the proposed IAEM for carrying out an elasto-plastic analysis for structures is efficient and accurate.

(1) Example 1: long span steel beam

The first example is a 16x40 wide flange section steel beam of 9.14 m span. The dimensions, supports, loading conditions, and cross section are shown in **Figure 5**. The beam has a modulus of elasticity of 205GPa and yield strength of 248MPa. The beam is loaded at one-third points along its span. With the IAEM, 24 general shaped elements are used including two boundary elements. However, 22,357 square elements with a constant thickness are required to model the same beam using original AEM while taking in consideration the variation in thickness for flanges and web. Based on IAEM analysis, the sequences plastic collapse mechanism of the beam and the formation of the plastic zones are shown in **Figure 6**.The results obtained by the proposed method (IAEM) are compared with those by Salmon[21]. The results are presented in vertical load versus deflection at the loaded point curve as shown in **Figure 7**. The comparison shows a very good agreement with the theoretical results.

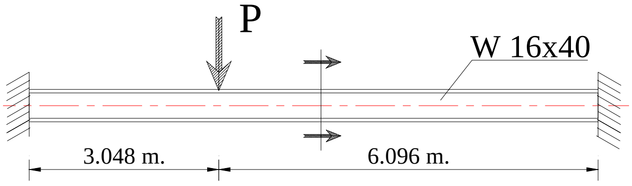

Figure 5 Long-span steel beam

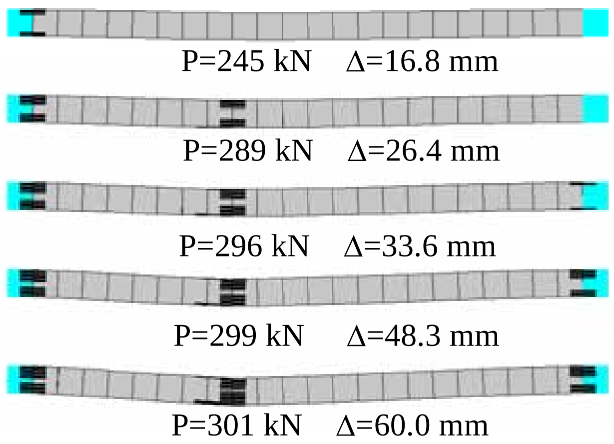

Figure 6 Formation of plastic zones

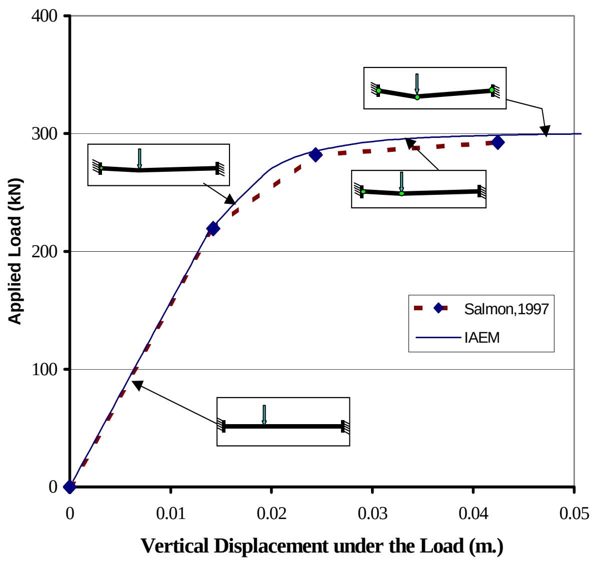

Figure 7 Ultimate load carrying capacity

(2) Example 2: Portal steel frame

The ultimate carrying capacity analysis for the rectangular portal frame (shown in **Figure 8**) had carried out. The frame was divided into 61 elements. The cross section and material properties of the members are listed in **Table 1**. The ultimate load capacity of the frame, according the experimental test that was carried out by Hodge[22] was 133.0kN. However, based on IAEM, the maximum frame resistance is reached at load (P) of 136kN which is around 2% higher than the maximum recorded load during the experiment. The load-vertical displacement curve obtained by both IAEM and the Rigid Body-Spring discrete element Method (RBSM) obtained by Ren[23] are plotted in **Figure 9** as well as the experimental data by Hodge[22]]. **Figure 10** shows the location of the developed plastic zones which are represented as dark areas in the figure. The results demonstrate the good agreement with experimental and RBSM results. Moreover, it can be also shown that unlike RBSM, the IAEM can follow the spread of yielding through the section. Therefore, it can capture member stability with enough accuracy for a wide range of beam-to-column problems.

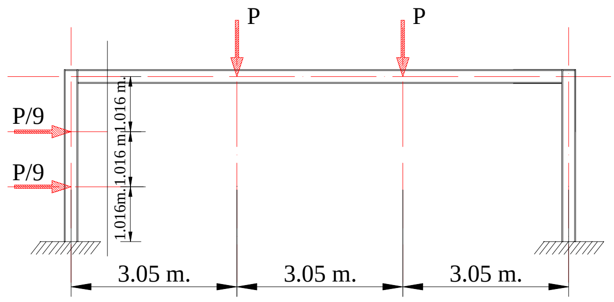

Figure 8 Analysis Model

Table 1 Cross-section and material properties of members

Area	(A)	0.645×10^{-2} m^2
Moment of inertia	(I)	1.0886×10^{-4} m^4
Yield strength	(Fy)	275.8 N/mm^2
Young's modulus	(E)	209 kN/mm^2
Poisson's ratio	(ν)	0.30

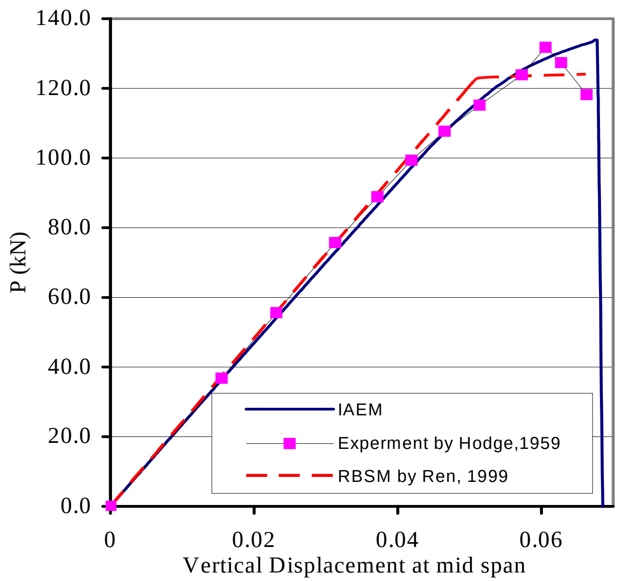

Figure 9 Ultimate load carrying capacity of the frame

Figure 10 Location of plastic hinges

5. COLLAPSE OF MULTI-STORY STEEL BUILDINGS

In this section, the IAEM is applied to investigate the validity of the proposed method in simulating progressive failure of steel structural buildings under hazardous load conditions. Concerning the collapse mechanisms of steel frames under severe ground motions, **Figure 11** shows four common patterns of failure for severely damaged buildings based on IAEM analysis. From the figure, main causes of building collapse are illustrated, included: the global plastic building collapse, collapse of intermediate floors and collapse of upper floors.

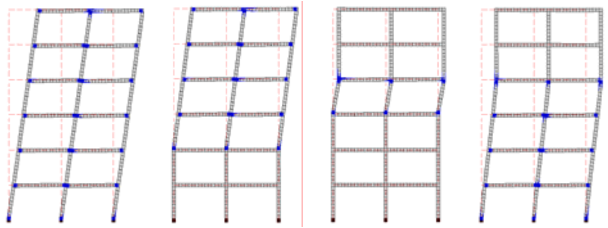

Figure 11 Failure modes of frames

A detailed analysis of the collapsing process of a multi-story steel structure under severe ground motion conditions is presented in this section.

(1) Structural model

The structure considered is a plane nine-story steel frame with three bays of 9.00m long, as illustrated in **Figure 12**. The typical height per story is 3.75m. The dimensions of the structural members are given in **Table 2**. In this frame, columns are bent about their major axes and rigid connections are assumed. The building was designed in accordance with the 1997 NEHRP recommended seismic provisions (Foutch[24)]). The steel is modeled as a bi-linear plastic material with a yield stress of 275 MPa and 355 MPa for beams and columns, respectively, and a strain hardening ratio of 4% of the elastic modulus. Young's modulus is taken as 205GPa. Rayleigh damping with 5% damping for the first fundamental mode is assumed. Using IAEM, only 477 elements are utilized for modeling the whole structure.

(2) Seismic response

The inelastic dynamic analysis has been performed, which integrates step-by-step the differential equations of motion corresponding to a given seismic input. Both material and geometric nonlinearity has been considered. Displacement time history analysis has been conducted of combined horizontal and vertical components of the first 40 seconds of the Hyogoken-Nanbu Earthquake (1995). The PGA of the horizontal component (KOBE/KJM000) was 813 gal and had a PGD of 17.68cm while the vertical component (KOBE/KJM-UP) had a peak ground acceleration of 336gal and a PGD of 10.29cm.

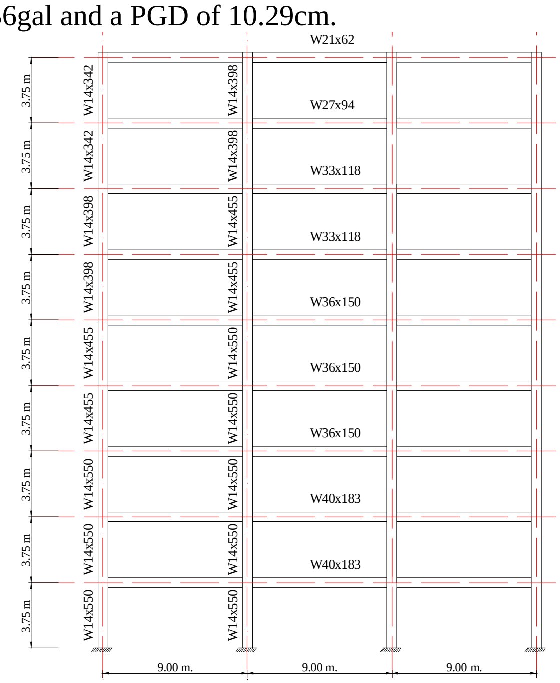

Figure 12 Nine-story steel frame

Table 2 Cross sections assigned for a 9-story steel building

Story	Columns		Beams
	Exterior	Interior	
9	w14x342	w14x398	w21x62
8	w14x342	w14x398	w27x94
7	w14x398	w14x455	w33x118
6	w14x398	w14x455	w33x118
5	w14x455	w14x550	w36x150
4	w14x455	w14x550	w36x150
3	w14x455	w14x550	w36x150
2	w14x550	w14x550	w40x183
1	w14x550	w14x605	w40x183

(3) Collapse analysis

The seismic response of the moment-resisting steel-frame structure had been preformed using IAEM. It had been shown from the analysis that however plastic hinges had been deformed at the end of all beam-to-column connections, the frame did not collapse. Therefore, a virtual structure will be used in this paper to illustrate a simulation of the building collapse under two different failure modes. The first failure is ground floor type failure as illustrated in **Figure 13**. In the virtual frame a reduction of 40 % of steel strength of the columns at ground level and lack of ductility in column-to-beam connections were assumed. The intense shaking caused the failure of load bearing columns in the lower floor level and cause progressive failure. According to the figure, firstly the ground motion excitation resulted in the formation of plastic hinges at several locations. The zones that have plastic deformation are represented by dark color in the figure. From the figure, it can be noted that most of the plastic hinges formed in beams, instated of columns, is due to the strong column-weak beam design philosophy. With the progress of time and formation of enough plastic hinges, the weakness of the strength and the low ductility demand of the ground floor level produced a failure in the ground floor columns. The end stage of the failure, illustrated in **Figure 13**, shows a good agreement with a recorded collapse case of multi-story steel buildings due to Hyogoken-Nanbu, Kobe Earthquake (1995) (as shown in **Figure 14**).

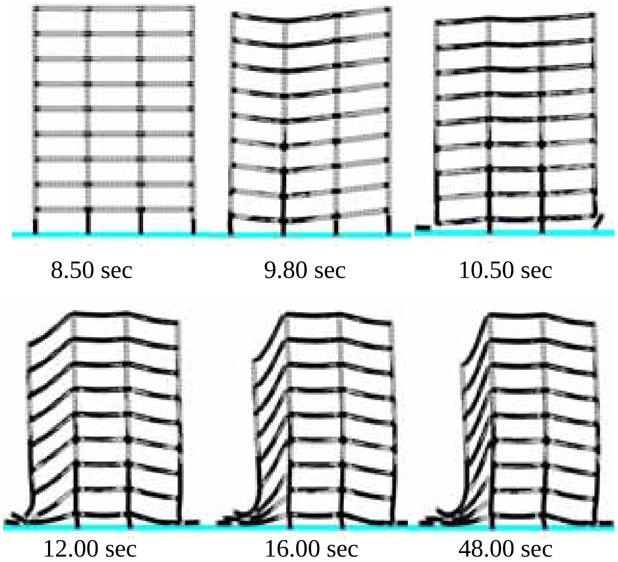

Figure 13 Soft–story damage at ground floor level

Figure 14 Ground-level soft-story collapsed building during Kobe Earthquake, 1995 (by K. Meguro)

Another well observed failure mode is the intermediate soft floor type of failure. This failure mechanism had been widely observed for many multi-story steel buildings due to the Kobe Earthquake (1995), as illustrated in **Figure 15**. The sequence of intermediate soft-story failure based on IAEM simulation is illustrated in **Figure 16**. The collapse had been initiated due to the same assumption of weakness of columns and reduction of ductility at intermediate floor level. The weakness of columns and the intensity of the ground motion develop inelastic behavior through the formation of yielding zones at the connections between beams and columns. Developing plastic zone hinges permit free lateral displacement of frame to occur and initiate the failure. The collapse process in **Figure 16** represents a progressive collapse type in which the collapse is propagating to several floors. A detailed analysis of effect of enhancing the connection ductility on the mitigation of this progressive collapse using IAEM is given in [25]. The results show that with certain ductility level the collapse may be stop at only one-story-collapse as shown in **Figure 15.**

Figure 15 Typical intermediate floor soft-story collapsed buildings during Kobe Earthquake, 1995 (by K. Meguro)

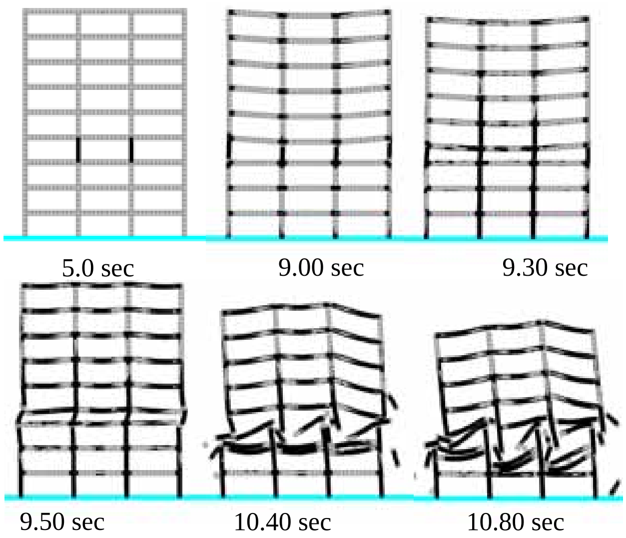

Figure 16 Soft–story damage at intermediate level

From the results, it can be concluded that the collapse of large scale structures due to earthquakes can be performed with sufficient accuracy by using the well-verified and calibrated analysis tool (IAEM). The calculation time required for the simulation of complete failure required only approximately one and half hours on a personal computer. This was due to the simplification of the IAEM which assumes a much less number of elements compared to traditional methods. Such a minimal requirement of computational time, with acceptable accuracy, can be considered as a unique advantage of this model.

6. CONCLUSIONS

This paper has attempted to briefly trace the development of the IAEM for analyzing the entire behavior of large scale steel structures up to total failure. The main feature of this tool is to use as few elements as possible to model each structural component and to obtain a realistic representation of material and geometric non-linearity. The results indicate that the improved method is capable of accurately analyzing the ultimate load-carrying capacity of steel structures. Numerical examples showing the accuracy, efficiency, and the range of application are presented. The program is a useful tool for performing intensive parametric studies to achieve a deeper understanding of structural behavior of steel structures under strong ground motions. Our method can help engineers to investigate the performance of even high-rise buildings under different hazardous loads such as fire[11)~13)], explosion[13)] and ground motions. The mechanism of progressive failure and the effect on the neighboring buildings can also be simulated.

REFERENCES

1) FEMA (2000) "Recommended seismic design Criteria for New Steel Moment-Frame Buildings." Report No. 350, FEMA, Washington, DC.
2) Miller, D. K. (1998) "Lessons learned from the Northridge earthquake." *Engineering Structures*, Vol. 20, 249-260.
3) Nakashima M., Inoue K., and Tada M. (1998) "Classification of Damage to Steel Buildings Observed in the 1995 Hyogoken-Nanbu Earthquake." *Engineering Structures*, Vol. 20, 271-281.
4) Holguin R., (1998) "Building Department's Response to EQ Damage to Steel Frame Buildings." *Journal of Performance of Constructed Facilities*, Vol. 12, No. 4, 199–201.
5) Toi, Y. and Yoshida, S. (1991) "Numerical Simulation of Nonlinear Behaviors of Two-Dimensional Block Structures." *Computers and Structures*, Vol. 41, No. 4, 593-603.
6) Meguro, K., Iwashita, K., and Hakuno, M. (1991) "Fracture Analyses of Structures by the Modified Distinct Element Method." *Structural Engineering and Earthquake Engineering*, Vol. 6, No. 2, 283–294.
7) Munjiza, A., Owen, D. R. J., and Bicanic, N. (1995) "A Combined Finite-Discrete Element method in Transient Dynamic of Fracturing Solids." *Engineering Computations*, Vol. 12, 145-174.
8) Meguro, K. and Tagel-Din, H. (2001) "Applied Element Simulation of RC Structures under Cyclic Loading." *ASCE*, Vol. 127 No. 11, 1295-1305.
9) Tagel-Din, H. and Meguro, K. (2000) "Applied Element Method for Dynamic Large Deformation Analysis of Structures." *Structural Engineering and Earthquake Engineering*, Vol.17, No. 2, 215-224.
10) Tagel-Din, H. and Meguro, K. (2000) "Analysis of a Small Scale RC Building Subjected to Shaking Table Tests using Applied Element Method." *Proceedings of the 12th WCEE*, New Zealand.
11) Elkholy, S. and Meguro K. (2003) "Dynamic Progressive collapse of High-Rise Buildings." *The 2nd International Symposium on New Technologies for Urban Safety of Mega Cities in Asia*, Tokyo, Japan, 323-330.
12) Elkholy, S., Tagel-Din, H., and Meguro K. (2003) "Structural Failure Simulation due to Fire by Applied Element Method." *The Fifth Japan Conference on Structural Safety and Reliability*, JCOSSAR, 47-52.
13) Elkholy, S. and Meguro, K. (2004) "Numerical modeling of steel structures in fire conditions using Improved Applied Element Method." *Proceedings of the 3rd International Symposium on New Technologies for Urban Safety of Mega Cities in Asia*, Kanpur, India.
14) Ramanchara, P. and Meguro K. (2002) "Nonlinear Static Modeling of Disp-Slip Fault for Studying Ground Surface Deformation using Applied Element Method." *Structural Engineering and Earthquake Engineering*, Vol. 9, No.2, 169-178.
15) Mayorca, P. and Meguro K. (2002) "Extension of the Applied Element Method for the Analysis of Masonry Structures." *Proceedings of the 4th International Summer Symposium*, JSCE: 41-44.
16) Giberson, M. F. (1969) "Two Nonlinear Beams with Definitions Ductility" *Journal of Structural. Division*, ASCE. Vol. 95, (ST2): 137-157.
17) Chen WF, Goto Y, Liew JYR. (1996) "Stability Design of Semi-Rigid Frames." *Wiley*, New York.
18) Liew JYR, White DW, Chen WF. (1993) "Second-order refined plastic hinge analysis for frame design: parts 1 and 2." *ASCE Journal of structural Engineering*, Vol. 119, No. 11, 3196-3237.
19) Chan, SL. (1989) "Inelastic post-buckling analysis of tubular beam-columns and frames," *Journal of Structural Engineering*, 11:23–30.
20) Clarke MJ. (1994) "Plastic zone analysis of frames." In: Chen WF, Toma S, editors. Advanced analysis of steel frames. Boca Raton, FL: CRC Press.
21) Salmon CG, and Johnson H. (1997) "Steel structures – design and behavior." Addison-Wesley Pub, 4th edition, , ISBN: 0673997863.
22) Hodge Jr PG. (1959) "Plastic analysis of structures." New York: McGraw-Hill.
23) Ren W., Tan X. and Zheng Z. (1999) "Nonlinear analysis of plane frames using rigid body-spring discrete element method", *Computers & Structures*, Vol.71, No. 1, 105-119.
24) Foutch, DA. And Yun SY. (2002) "Modeling of Steel Moment Frames for seismic loads." *Journal of Constructional Steel Research*, Vol. 58, Issue (5-8),529-564.
25) Elkholy, S. (2004) "Improved Applied Element Method for Numerical Simulation of Structural Failure and Collapse." *PhD Dissertation*, Department of Civil Engineering, Tokyo University, Japan.

(Received March 15, 2005)